ELSEVIER

Journal of Organometallic Chemistry 656 (2002) 188–198

Journal of Organometallic Chemistry

www.elsevier.com/locate/jorganchem

Synthesis and characterisation of derivatives of $[HIr_4(CO)_{10}(\mu\text{-}PPh_2)]$ with mono and diphosphines; X-ray molecular structures of $[HIr_4(CO)_8(PPh_3)_2(\mu\text{-}PPh_2)]$ and $[HIr_4(CO)_8\{Ph_2P(CH_2)_nPPh_2\}(\mu\text{-}PPh_2)]$ ($n = 1$ and 4)

Cláudio M. Ziglio [a], Maria D. Vargas [a,*], Dario Braga [b], Fabrizia Grepioni [b], John F. Nixon [c]

[a] *Instituto de Química, Universidade Estadual de Campinas, CP 6154, Campinas 13083-970, SP, Brazil*
[b] *Dipartimento di Chimica 'G.Ciamician', Universitá degli Studi di Bologna, Via Selmi 2, 40126 Bologna, Italy*
[c] *School of Chemistry, Physics and Environmental Science, University of Sussex, Brighton BN1 9QJ, UK*

Received 18 March 2002; received in revised form 13 May 2002; accepted 13 May 2002

Abstract

The reactions of the cluster compound $[HIr_4(CO)_{10}(\mu\text{-}PPh_2)]$ (**1**) with a series of phosphines, PMe_3 and PPh_3, and diphosphines, $Ph_2P(CH_2)_nPPh_2$ ($n = 1$, dppm, $n = 2$, dppe and $n = 4$, dppb) and *cis*-$PPh_2CH{=}CHPPh_2$ (dppen), have been investigated. Reaction of **1** with PMe_3 yielded the mono and di-substituted derivatives $[HIr_4(CO)_{10-n}(PMe_3)_n(\mu\text{-}PPh_2)]$ ($n = 1$, **2** and $n = 2$, **3**). ^{1}H and ^{31}P-NMR spectroscopy monitoring revealed that the two kinetic isomers **2b** and **2c** undergo conversion to the thermodynamic isomer **2a** through a process, which apparently involves intra-molecular migration of the PMe_3 ligand. In contrast, analogous kinetic isomers were not detected during the synthesis of the PPh_3 derivative $[HIr_4(CO)_9(PPh_3)(\mu\text{-}PPh_2)]$ (**4**). According to ^{1}H and ^{31}P-NMR data, compounds $[HIr_4(CO)_8(L)_2(\mu\text{-}PPh_2)]$ (L = PMe_3 **3** and PPh_3 **5**) exist in solution in three isomeric forms **3a**–**3c** and **5a**–**5c**, respectively, at −60 °C. Compound **1** also reacts with diphosphines to give CO substitution products, whose composition depends on the size of the methylene chain. Whilst reaction with dppm and dppen yields only the bi-substituted species $[HIr_4(CO)_8(dppm)(\mu\text{-}PPh_2)]$ (**6**) and $[HIr_4(CO)_8(dppen)(\mu\text{-}PPh_2)]$ (**7**), respectively, with dppb, both the dimeric compound $[\{HIr_4(CO)_9(\mu\text{-}PPh_2)\}_2(dppb)]$ (**8a**) and the monomeric species $[HIr_4(CO)_8(dppb)(\mu\text{-}PPh_2)]$ (**8b**) are formed, and with dppe, only the dimeric compound $[\{HIr_4(CO)_9(\mu\text{-}PPh_2)\}_2(dppe)]$ (**9**) is obtained. The dppm derivative exists in solution in the form of two inter-converting isomers **6a** and **6b** that differ with respect to the mode of coordination of the dppm and CO ligands. Isomerisation of **6a**–**6b** is proposed to involve intra-molecular migration of dppm and carbonyl ligands. Structures were proposed for all compounds, on the basis of ^{1}H and ^{31}P[^{1}H]-NMR studies and of correlations previously established for the phosphine and diphosphine derivatives of $[Ir_4(CO)_{12}]$; the molecular structures of compounds **5c**, **6a** and **8b** were established by X-ray diffraction studies which confirmed the structures proposed based on spectroscopic data.

Keywords: Cluster; Iridium; Phosphines; Carbonyl; Isomerisation

1. Introduction

The reactions of $[HIr_4(CO)_{10}(\mu\text{-}PPh_2)]$ (**1**) with a series of phosphines L = $P(p\text{-}C_6H_4X)_3$ (X = F, Cl, H, Me and OMe) were reported previously [1]. Even in the presence of excess phosphine L, the mono-substituted species $[HIr_4(CO)_9L(\mu\text{-}PPh_2)]$ were the dominant products from these reactions and were isolated in yields up to 95%. The molecular structures of **1** and of the PPh_3 derivative were determined by X-ray analyses and shown to be very similar, the difference being the presence of a PPh_3 ligand in place of an axial CO on a base iridium atom not associated with the PPh_2 ligand. The di-substituted products $[HIr_4(CO)_8L_2(\mu\text{-}PPh_2)]$ were isolated, albeit in low yields, and characterised only by IR and ^{1}H-NMR spectroscopy.

* Corresponding authors. Fax: +55-19-3788-3023
E-mail address: mdvargas@iqm.unicamp.br (M.D. Vargas).

0022-328X/02/$ - see front matter
PII: S0022-328X(02)01583-8

Our recent studies indicate that the mono and di-substituted phosphine derivatives of **1** behave differently from **1** in the presence of molecules or fragments that may undergo oxidative addition [2–4]. Although **1** does not react with alkynes and alkenes [5], phosphines containing unsaturated fragments, such as $Ph_2PC{\equiv}CPh$, can interact further with **1** to yield μ_4-η^3-Ph_2PCCPh containing species and products resulting from P–C bond activation [6,7], further hydrometallation [8] or P–C bond formation [9]. We, therefore, decided to synthesise a number of phosphine and diphosphine derivatives of **1**, in order to study the steric and electronic effects of the phosphines on the reactivity of the substituted species. The synthesis and characterisation of a series of phosphine and diphosphine derivatives are reported below and the oxidative addition reactions of these species will be described in other papers [3,4].

2. Results and discussion

2.1. Synthesis and characterisation of $[HIr_4(CO)_9(PMe_3)(\mu\text{-}PPh_2)]$ (**2**) and $[HIr_4(CO)_8(PMe_3)_2(\mu\text{-}PPh_2)]$ (**3**)

Compounds **2** and **3** were obtained in 50 and 20% yields, respectively, from the reaction of $[HIr_4(CO)_{10}(\mu\text{-}PPh_2)]$ (**1**) with one equivalent of PMe_3 in toluene, whilst compound **3** was produced in high yields, above 90%, from the reaction of **1** with two equivalents of PMe_3, under argon. The two compounds are red crystalline solids, soluble in common organic solvents and air stable in the solid state.

All attempts to produce only the mono-substituted compound in high yield, as described for the reactions with other phosphines, such as PPh_3 [1], were unsuccessful. Kinetic studies have shown that the reactions of **1** with $P(p\text{-}C_6H_4X)_3$ (X = F, Cl, H, Me and OMe), to give the mono-substituted derivatives, proceed via an associative mechanism [10]. In these cases, the substitution of a second CO is a slow process, only noted after periods of time longer than 3 half lives, under pseudo-first order conditions. Considering that PMe_3 is more basic and has a much smaller cone angle than all $P(p\text{-}C_6H_4X)_3$, the large increase in the CO substitution rate, after the substitution of the first CO ligand with PMe_3, would be expected if the process occurs, also in this case, via an associative mechanism.

Compound **2** was characterised by analytical (experimental) and spectroscopic data (Tables 1 and 2).

Monitoring of the reaction of **1** with PMe_3 by ^{31}P-NMR spectroscopy revealed formation of three products **2a**–**2c**, whose relative concentrations changed drastically with time and which could not be separated from each other by TLC. Comparison of the ^{31}P-NMR spectra of the mixture containing **2a**–**2c** shortly after purification by TLC and after 3 h standing in C_6D_6 showed that isomers **2b** and **2c** had transformed into **2a**, which indicated that **2b** and **2c** were the kinetic products of the reaction and **2a** the thermodynamic one. No evidence was found for the formation of similar intermediate kinetic products in the reactions of **1** with $P(p\text{-}C_6H_4X)_3$. Thus, it is possible that the lack of site selectivity observed in the reaction of **1** with PMe_3 is related both to the small cone angle of this phosphine [105°, compared with 145°, for $P(p\text{-}C_6H_4X)_3$] and to its high basicity [pK_a 8.65, compared with 1.0–4.6, for $P(p\text{-}C_6H_4X)_3$], that would favour nucleophilic attack at the cluster.

Table 1
Infrared data in the ν_{CO} region of some derivatives of $[HIr_4(CO)_{10}(\mu\text{-}PPh_2)]$ (**1**) [a]

Cluster	ν_{CO} (cm^{-1})
$[HIr_4(CO)_9(PMe_3)(\mu\text{-}PPh_2)]$ (**2a**–**2c**)	2072 m, 2042 vs, 2033 s, 2014 m, 2007 m, 1996 m, 1835 w (br), 1812 w (br)
$[HIr_4(CO)_8(PMe_3)_2(\mu\text{-}PPh_2)]$ (**3a**–**c**)	2070 vw, 2039 s, 2008 vs, 1975 vs, 1961 s, 1948 s, 1814 m (br), 1795 m (br)
$[HIr_4(CO)_8(PPh_3)_2(\mu\text{-}PPh_2)]$ (**5**) [b]	2064 vs, 2023 vs, 1985 vs, 1997 m (sh), 1976 m (sh),1803 w (br), 1734 vw (br)
$[HIr_4(CO)_8(dppm)(\mu\text{-}PPh_2)]$ (**6a**) [b]	2044 w, 2011 s, 1980 w (sh)
$[HIr_4(CO)_8(dppm)(\mu\text{-}PPh_2)]$ (**6b**) [b]	2056 vs, 2022 s, 1992 s, 1975 m (sh), 1787 w (br)
$[HIr_4(CO)_8(dppen)(\mu\text{-}PPh_2)]$ (**7**)	2056 s, 2024 vs, 1992 s, 1969 m, 1945 m
$[\{HIr_4(CO)_9(\mu\text{-}PPh_2)\}_2$-(dppb)] (**8a**)	2070 s, 2033 vs, 2006 s, 1996 m, 1978 m, 1813 w (br)
[HIr4(CO)8(dppb)(μ-PPh_2)] (**8b**)	2060 vs, 2024 s, 1999 s, 1974 m, 1823 w (br)
$[\{HIr_4(CO)_9(\mu\text{-}PPh_2)\}_2$-(dppe)] (**9**)	2070 s, 2040 s, 2032 vs, 2006 s, 1998 m, 1972 m, 1735 w (br)

[a] Measured in hexane unless otherwise stated.
[b] Measured in CH_2Cl_2.

The IR spectrum of the **2a**–**2c** mixture in the ν_{CO} region (see Table 1) displays three characteristic bridging CO bands, confirming the presence of a bridging CO in the three isomers. The room temperature ^{1}H and ^{31}P[^{1}H]-NMR spectra of the **2a**–**2c** mixture (see Table 2) indicate that the three compounds have very similar structures, with the same basic frame as compound **1**, differing only with respect to the PMe_3 position on the metal tetrahedron. The ^{1}H-NMR spectrum shows low frequency signals assigned to the bridging hydride ligands *transoid* to the phosphorus PPh_2 in **2a**–**2c**. The ^{31}P[^{1}H]-NMR spectrum exhibits high frequency signals which are assigned to the bridging phosphido phosphorus, and the PMe_3 phosphorus signals at low frequency. The PMe_3 ligand could, in principle, occupy any of the nine terminal CO positions in **1**, indicated in Scheme 1.

The room temperature ^{13}C-NMR spectrum of compound **2a**, obtained from a ^{13}CO enriched sample,

Table 2
$^{31}P[^{1}H]$ and ^{1}H-NMR data of some of the derivatives of **1**

Cluster	δ $^{31}P\{^{1}H\}$ (ppm), J (Hz)	δ ^{1}H (ppm), J (Hz)
2 [a]	−48.1(d, J_{P-P} 10, PMe_3), 279.5(br, PPh_2), **2a**; −62.1(d, J_{P-P} 11, PMe_3), 273.1 (d, PPh_2), **2b**; −51.7 (br, PMe_3), 256.7 (br, PPh_2), **2c**	−12.7 (d, J_{H-P} 56, μ-H), **2a**; −12.5 (d, J_{H-P} 55, μ-H), **2b**; −12.8 (d, J_{H-P} 52, μ-H), **2c**;1.0–1.5 (m, CH_3), 7.0–8.0 (m, Ph)
3 [a]	−71.3 (d, J_{P-P} 11, PMe_3), −46.8 (s, PMe_3), 271.7 (br, PPh_2), **3a**; −51.7 (d, J_{P-P} 10, PMe_3), −42.5 (s, PMe_3), 250.1 (br, PPh_2), **3b**; −78.9 (d, J_{P-P} 11, Pme_3), −51.1 (d, J_{P-P} 4,PMe_3), 266.9 (br, PPh_2), **3c**	−13.0 (d, J_{H-P} 57, μ-H), **3a**; −12.5 (d, J_{H-} 56, μ-H), **3b**; −12.2 (dd, J_{H-P} 54 e 4, μ-H) **3c**; 1.6–1.8 (m, CH_3), 6.9–7.7 (m, Ph)
5 [b]	−26.2 (d, J_{P-P} 4, PPh_3), −4.0 (s, PPh_3),262.4 (br, PPh_2), **5a**; −12.6 (s, PPh_3), −2.3(s, PPh_3), 272.6 (s, PPh_2), **5b**; −0.9 (s, PPh_3), 14.4 (s, PPh_3),259.4 (s, PPh_2), **5c**	−11.8 (d, br, J_{H-P} 55, μ-H), **5a**; −10.7 (d, br, J_{H-P} 51, μ-H), **5b**; −10.9 (ddd, J_{H-P} 75, 8, 4, μ-H), **5c**; 7.0–8.0 (m, Ph)
6 [a]	−69.4 (dd, J_{P-P} 38 and 10, dppm), −35.5 (dd, J_{P-P} 74 and 38, dppm), 273.3 (dd, J_{P-P} 74, 10, PPh_2), **6a**; −36.8 (dd, J_{P-P} 37 and 3,9, dppm), −31.5 (dd, 37, 3.6, dppm), 280.2 (br, PPh_2), **6b**	−14.3 (dd, J_{P-H} 41, 14 μ-H), 7.0–8.0 (m, Ph), **5a**; −10.8(ddd, J_{P-H} 53, 14, 7, μ-H), 7.0–8.0 (m, Ph), **5b**
7 [b]	31.5 (dd, J_{P-P} 11, 11, *dppen*), 43.0 (dd, 82 e 11), 262(dd, PPh_2)	−14.6 (ddd, J_{H-P} 41, 7.3, 7.1), 7.0–8.0 (m, Ph)
8a [b]	−5.0 (s, dppb), 280.8 (s, PPh_2)	−12.1 (dd, J_{H-P} 56 e 6, μ-H), 7.1–7.7 (m, Ph)
8b [b]	0.25 (s, dppb), 3.6 (s, dppb), 261.1 (s, PPh_2)	−12.2 (d, br, J_{H-P} 61, μ-H), 6.9–7.6 (m, Ph)
9 [b]	−3.3 (s, dppe) 284.3 (s, PPh_2)	−12.2 (d, br, J_{P-H} 56.4, μ-H), 7.0–7.7 (m, Ph)

[a] Measured in $CDCl_3$ at room temperature unless otherwise stated.
[b] Measured in CD_2Cl_2 at −40 °C.

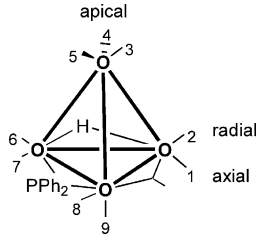

Scheme 1.

displays three very broad signals at δ 167.5, 162.4 and 164.2, but on cooling the signals begin to split below +10 °C, which clearly shows that the carbonyl ligands are involved in a fluxional process on the metal framework. At −60 °C the spectrum appears clearly defined and shows the nine resonances due to the carbonyl groups at δ 158.1 (s), 158.9 (d, J_{C-P} 25.5 Hz), 159.5 (s), 163.9 (s), 164.2 (s), 165.2 (s), 166.4(s), 183.6 (dd, J_{C-P} 12, 13 Hz) and 196.8 (d, J_{C-P} 35 Hz).

The ^{13}C-NMR spectrum of **2a** exhibits a very similar pattern to that of the analogous PPh_3 derivative **4**, at −60 °C, for which the phosphine ligand was shown to be bonded in the axial position by an X-ray analysis [1]. This result suggests that compounds **2a** and **4** are structurally identical and exhibit the structure shown on Scheme 2.

It was impossible to have enough ^{13}CO enriched **2b** and **2c** for VT ^{13}C-NMR studies, as both compounds rapidly isomerise to **2a**. The structures of isomers **2b** and **2c** were, therefore, proposed, based on analyses of the relative ^{31}P chemical shifts of the PMe_3 ligand and on comparisons with results reported on the solution structures of $[Ir_4(CO)_{12-n}L_n]$ ($L = PR_3$, $n = 1$–4), in which the PR_3 ligand may also occupy either axial, radial or apical positions. Indeed, this comparison seemed plausible because the basic structure of compounds **2a**–**2c** is related to that of the mono-substituted derivatives $[Ir_4(CO)_{11}L]$ (L = phosphines), with the bridging hydride and phosphide ligands in **2a**–**2c** in place of two bridging carbonyls in $[Ir_4(CO)_{11}L]$.

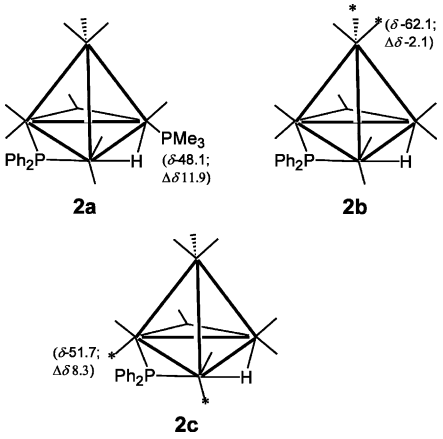

Scheme 2. Possible arrangements of the PMe_3 ligand in the mono-substituted derivatives of **1** $[HIr_4(CO)_9(PMe_3)(\mu\text{-}PPh_2)]$ (**2**) (* indicates a possible coordination site for the PMe_3 ligand).

As shown in Table 3, the coordination chemical shift, $\Delta\delta$ ($\delta_{coordinated} - \delta_{free\ ligand}$), for the axial positions on $[Ir_4(CO)_{12}]$ derivatives is considerably lower (values close to zero or slightly negative) than for the radial position (values largely positive), independently of the phosphine. In the $[Ir_4(CO)_8(PPh_2Me)_4]$ cluster [11], the phosphines occupy axial, radial and apical positions and it was shown that the apical $\Delta\delta$ is lower than the other two. These observations indicate the following sequence for the phosphine chemical shifts in iridium tetrahedral clusters: radial > axial > apical.

The coordination chemical shift of the minor isomer **2c** ($\Delta\delta$ 8.3) is similar to that of the major isomer **2a** ($\Delta\delta$ 11.9), which suggests that in **2c** the phosphine ligand

Table 3
^{31}P chemical shifts, δ, and coordination chemical shifts, $\Delta\delta$ ($=\delta_{coordinated}-\delta_{free\ ligand}$), for some $[Ir_4(CO)_{12}]$ derivatives

	δ Free	Axial		Radial		Apical	
		δ	$\Delta\delta$	δ	$\Delta\delta$	δ	$\Delta\delta$
$[Ir_4(CO)_{11}L]$							
L = PEt_3 [12]	−19.1	6.0	25.1	28.7	47.8	–	–
$PPhMe_2$ [13]	−45.4	−45.3	0.1	−24.2	21.3	–	–
PPh_2Me [11,13]	−28.1	−32.2	−4.1	−10.7	17.4	–	–
$PPhH_2$ [14]	−122.0	−124.5	−2.5	−81.0	41	–	–
	−41.1	−57.5	−16.4	−16.5	24.6	–	–
$[Ir_4(CO)_{10}L_2]$							
L = $PphMe_2$ [13]	−45.4	−44.8	0.6	−26.2	19.2	–	–
PPh_2Me [11,13,16]	−28.1	−28.8	−0.7	−6.7	21.4	–	–
PPh_3 [11,13]	−6.9	−14.0	−7.1	18.9	25.8	–	–
$[Ir_4(CO)_9LL']$							
L = $PphMe_2$, L′ = nbd [15]	−45.4	−51.5	−6.1	−27.2	18.2	–	–
L = PPh_2Me, L′ = nbd [15,16]	−28.1	−37.4	−9.3	−8.9	19.2	–	–
L = PPh_3, L′ = cod [15]	−6.9	−17.3	−10.4	21.0	27.9	–	–
L = PPh_3, L′ = cot [15]	−6.9	−17.7	−10.8	19.5	26.4	–	–
L = PPh_3, L′ = diars [16]	−6.9	−3.0	1.5	25.6	30.1	–	–
$[Ir_4(CO)_9L_3]$							
L = PPh_2Me [11]	−28.1	−25.0	3.1	−5.2	22.9	–	–
PPh_3 [11]	−6.9	−17.4	−10.5	20.0	26.9	–	–
$[Ir_4(CO)_7LL'_2]$							
L = PPh_2Me, L′ = nbd [15]	−28.1	−38.9	−10.8	−8.8	19.3	–	–
L = PPh_3, L′ = cod [15]	−6.9	−22.5	−15.6	25.5	32.4	–	–
$[Ir_4(CO)_8L_4]$							
L = PPh_2Me [11]	−28.1	−39.8	−11.7	−7.4	20.7	−59.9	−31.8

occupies one of the two remaining axial sites of the polyhedron as proposed in Scheme 2. On the other hand, the coordination chemical shift for the isomer **2b** phosphine ($\Delta\delta$ −2.1) is substantially lower compared with that observed for the other two isomers, suggesting that the ligand is located in an apical position in **2b**. The J_{P-P} coupling observed between the PMe_3 and PPh_2 ligands (11 Hz) in **2b** indicates that the two phosphorus nuclei are located in a *transoid* orientation, which is possible if the phosphine occupies sites 4 or 3 (see Schemes 1 and 2).

It is very probable that isomerisation of **2b** and **2c** into **2a** involves a change in the PMe_3 ligand coordination site, rather than migration of the hydride and phosphide ligands. This isomerisation may happen, either via PMe_3 migration from the previous site across the Ir–Ir bond to the more stable basal site without dissociation, or via PMe_3 dissociation and re-association [17], after scrambling of the CO groups. The intramolecular mechanism was first proven to be operative in the isomerisation of the platinum cluster $[Pt_3(\mu_3\text{-}CO)(\mu\text{-}Ph_2PCH_2PPh_2)_3L][PF_6]_2$ [18,19] and then of $[Pt_3(\mu_3\text{-}H)(\mu\text{-}Ph_2PCH_2PPh_2)_3L][PF_6]_2$ [20] (L = phosphines and phosphites) and involves migration of the ligand L around the triangular face of these clusters; it has also been proposed in the case of the isomerisation of the mixed metal clusters $[PPN][Fe_2Co(CO)_8(PR_3)(COO)]$ [21], $[Ir_3Rh(CO)_{11}(PPh_3)]$ [22] and $[Ir_2Rh_2(CO)_{11}(PPh_3)]$, [23] for which the authors suggest formation of a bridging PPh_3 containing transition state. Isomerisation of **2b** and **2c** into **2a** probably occurs via this mechanism.

Compound **3** was characterised by spectroscopic and analytical data (see Tables 1 and 2). The room temperature ^1H and $^{31}P[^1H]$-NMR spectra of compound **3** (see Table 2) show the presence of three similar sets of signals in an approximate 8:5:1 ratio, attributed to three isomeric forms (**3a**–**3c**) of the di-substituted derivatives of **1**. The relative ratio of these species stays unchanged when the solution is stored for days under argon and when it is heated up to 70 °C for several hours.

These NMR data indicate that the basic frame of isomers **3a**–**3c** is similar to those exhibited by compounds **1** and **2a**–**2c** (see Table 2). One of the PMe_3 resonances in isomers **3a** ($\Delta\delta$ 13.2) and **3c** ($\Delta\delta$ 8.9) appears close to the axial PMe_3 resonance in isomers **2a** ($\Delta\delta$ 11.9) and **2c** ($\Delta\delta$ 8.3), respectively. These data suggest that in the di-substituted derivatives **3a** and **3c** one of the PMe_3 ligands occupy the same position as in

the mono-substituted **2a** and **2c**, respectively. The chemical shifts of the second PMe_3 in isomers **3a** and **3c** appear at low frequency ($\Delta\delta$ −11.3 and −18.9, respectively), relative to the axial PMe_3. On the basis of the chemical shift sequence described above for $[Ir_4(CO)_{12}]$ derivatives (Table 3) the second PMe_3 probably occupies an apical position in isomers **3a** and **3c** (see Scheme 3). For both isomers, a coupling between the PMe_3 and PPh_2 ligands (11 Hz) is observed, indicating that the phosphine phosphorus nucleus in each compound occupies either apical sites 4 or 3, which are located *transoid* to the phosphide phosphorus (see Scheme 1).

The PMe_3 resonances in isomer **3b** are closer to those observed for isomers **2a** and **2c**, suggesting the axial–axial arrangement of the PMe_3 ligands illustrated in Scheme 3. Similarly to the mono-substituted derivative **2c**, it is impossible, based only on NMR data, to be sure to which of the two Ir atoms bridged by the phosphide group the second axial PMe_3 ligand is bonded (see Scheme 3).

2.2. Synthesis and characterisation of $[HIr_4(CO)_8(PPh_3)_2(PPh_2)]$ (5)

The synthesis of **5** from the reaction of **1** with an excess of PPh_3 was reported to give low yields of the product [1]. Much better yields of **5** (up to 80%) were obtained when the reaction of **4** with one equivalent of PPh_3 was carried out in the presence of equimolar amounts of Me_3NO, which decarbonylates compound **4**. The red compound **5** was characterised by spectroscopic and analytical methods, and an X-ray analysis was carried out on one of its isomers.

The ^1H and $^{31}P[^1H]$-NMR spectra of compound **5** (see Table 2), at −40 °C, show the presence of three similar sets of signals in an approximate 4:1:8 ratio, attributed to three isomeric forms (**5a**–**5c**). Similarly to the analogous **3**, the relative ratio of these species stays unchanged when the solution is stored for days under argon and when it is heated to up to 70 °C for several hours. In all isomers a PPh_3 resonance appears close to the PPh_3 resonance observed in the mono-substituted derivate **4** (Table 2), which is known to be located in an axial site as illustrated in Scheme 4 [1] thus suggesting that the three isomers differ only with respect to the position of the second PPh_3 ligand. Since the resonance of the second PPh_3 in isomer **5a** appears at lower frequency than the signal of the axial phosphine, it may be bonded in an apical position (see Scheme 4). Isomer **5b** also exhibits the resonance of the second PPh_3 at a frequency lower than that of the axial phosphine, however, in this case the difference is less significant, suggesting that this ligand occupies another axial position, as proposed in Scheme 4. These assignments indicate that isomers **5a** and **5b** are structurally similar to the analogous PMe_3 containing **3a** and **3b** (compare Schemes 3 and 4). Isomer **5c**, however, is not similar to **3c**, i.e. the phosphine ligands in the two compounds are distributed in a different arrangement on the metal polyhedron. The resonance of the second PPh_3 ligand in **5c** appears in higher frequency than the signal of the axial PPh_3, indicating a radial coordination. The structure proposed for isomer **5c** on the basis of ^{31}P-NMR data was confirmed by a single-crystal X-ray diffraction study (see below).

2.2.1. Crystal and molecular structure of 5c

The molecular structure of compound **5c** is shown in Fig. 1. The description of this structure will involve comparisons with the structures of compounds **1** and **4**, reported previously, and, therefore, selected bond

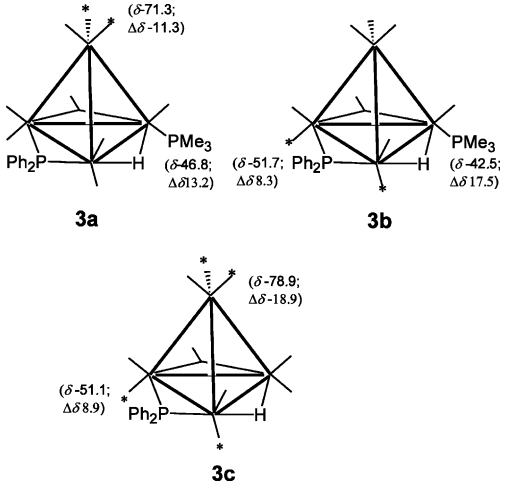

Scheme 3. Possible arrangements of the PMe_3 ligands in di-substituted derivatives of **1**, $[HIr_4(CO)_8(PMe_3)_2(\mu\text{-}PPh_2)]$ (**3**) (* indicates a possible coordination site for PMe_3 ligand).

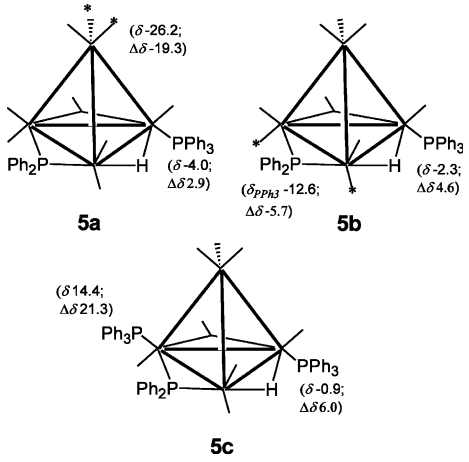

Scheme 4. Possible arrangements of the PPh_3 ligands in di-substituted derivatives of **1** (* indicates a possible coordination site for PPh_3 ligand).

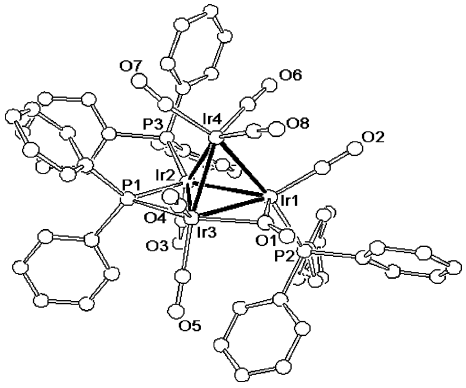

Fig. 1. Molecular structure of $[HIr_4(CO)_8(PPh_3)_2(\mu\text{-}PPh_2)]$ (**5c**).

lengths and angles for these compounds are also listed in Table 4.

The structures of the three compounds exhibit similar distorted tetrahedral arrangements of Ir atoms with the basal edges bridged by a hydride, a carbonyl and a phosphide ligands. The Ir–Ir distances in the three molecules follow the same trends in the three structures. The three basal edges are longer than the three unbridged apex to base edges. In particular, as in the other Ir_4 clusters, instead of the expected shortening of the Ir–Ir edge associated with a bridging carbonyl, in all three clusters, the Ir(1)–Ir(3) edge is longer than the unbridged edges. A substantial increase in the average Ir–Ir bond distances is induced by the presence of the terminally bound PPh_3 ligands in **4** and **5c**. Also, the axial PPh_3 on basal Ir(1) in compound **4** leads to a larger asymmetry of the bridging carbonyl [Ir(1)–C(1) 1.95(5), Ir(3)–C(1) 2.27(4)], compared with **1** [Ir(1)–C(1) 1.92(4), Ir(3)–C(1) 2.14(4)], which is probably the result of the increase in the electron density on Ir(1) and thus more effective $Ir(1)\pi \rightarrow C(1)$ donation. The presence of the second PPh_3 on an equatorial site of basal Ir(2) in compound **5c** restores, somehow, the electronic balance.

2.3. Synthesis and characterisation of $[HIr_4(CO)_8(dppm)(\mu\text{-}PPh_2)]$ (**6a–6b**)

The reaction of compound **1** with one equivalent of dppm in CH_2Cl_2 produces two compounds, red **6a** and yellow **6b**, in 30 and 20% yields, respectively, after separation on TLC plates.

Compounds **6a** and **6b** were characterised by spectroscopic and analytical data, as shown in Tables 1 and 2. The IR spectra of the two compounds in the ν_{CO} region in CH_2Cl_2 (see Table 1), obtained just after TLC separation and after standing in solution for 12 h, Fig. 2, show that the two compounds undergo inter-conver-

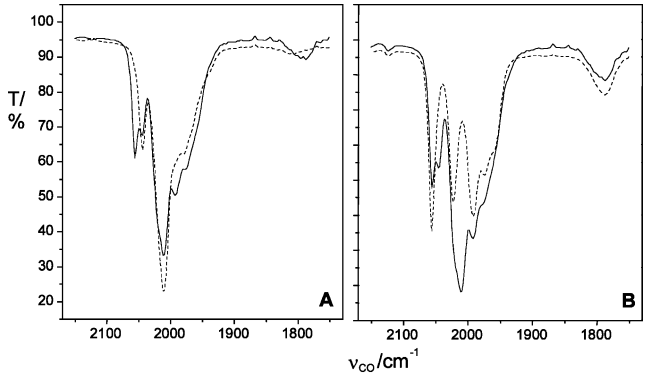

Fig. 2. IR spectra (ν_{CO} region) of isomers **6a** (A) and **6b** (B) at t_0 (dashed line) and $t_f = 12$ h (solid line), in CH_2Cl_2.

Table 4
Selected bond distances (Å) and angles (°) for compounds $[HIr_4(CO)_{10}(\mu\text{-}PPh_2)]$ (**1**), [1] $[HIr_4(CO)_9(PPh_3)(\mu\text{-}PPh_2)]$ (**4**), [1] $[HIr_4(CO)_8(PPh_3)_2(\mu\text{-}PPh_2)]$ (**5c**), $[HIr_4(CO)_8(dppm)(\mu\text{-}PPh_2)]$ (**6a**) and $[HIr_4(CO)_8(dppb)(\mu\text{-}PPh_2)]$ (**8b**)

	1	**4**	**5c**	**6a**	**8b**
Ir(1)–Ir(2)	2.769(2)	2.785(2)	2.810(1)	2.890(1)	2.857(2)
Ir(1)–Ir(3)	2.735(2)	2.771(2)	2.762(1)	2.696(2)	2.754(2)
Ir(1)–Ir(4)	2.677(2)	2.706(2)	2.691(1)	2.701(1)	2.693(2)
Ir(2)–Ir(3)	2.797(2)	2.802(2)	2.815(1)	2.703(2)	2.829(2)
Ir(2)–Ir(4)	2.712(2)	2.719(2)	2.755(1)	2.733(1)	2.740(1)
Ir(3)–Ir(4)	2.734(2)	2.724(2)	2.730(1)	2.726(1)	2.736(2)
Ir(2)–P(1)	2.292(10)	2.311(11)	2.299(3)	2.315(4)	2.265(3)
Ir(3)–P(1)	2.342(11)	2.289(9)	2.327(3)	2.276(4)	2.328(3)
Ir(1)–P(2)		2.342(10)	2.310(3)	2.310(4)	2.310(3)
Ir(2)–P(3)			2.305(3)		2.336(2)
Ir(4)–P(3)				2.335(4)	
Ir(1)–C(1)	1.92(4)	1.95(5)	1.954(13)		1.956(9)
Ir(3)–C(1)	2.14(4)	2.27(4)	2.187(13)		2.192(9)
Ir(2)–P(1)–Ir(3)	74.2(3)	75.0(3)	74.97(10)	72.1(1)	76.03(9)
P(1)–Ir(3)–Ir(1)	112.1(2)	112.8(3)	112.49(8)	119.3(1)	112.51(8)
Mean [a] Ir–Ir	2.737_{42}	2.751_{40}	2.761_{47}	2.742_{74}	2.768_{62}
Mean Ir_{apical}–I_{basal}	2.707_{29}	2.716_{9}	2.725_{32}	2.720_{17}	2.723_{26}
Mean Ir_{basal}–Ir_{basal}	2.767_{31}	2.786_{16}	2.799_{29}	2.763_{110}	2.813_{53}

[a] Mean S.D. as subscript values.

sion. The spectra of the two solutions after 12 h (t_f) are identical and exhibit bands due to the two compounds. Only the spectrum of isomer **6b** exhibits a bridging CO band, at 1787 cm^{-1}, indicating that all CO groups in **6a** are coordinated in a terminal mode.

The inter-conversion process was confirmed by ^{1}H and ^{31}P spectroscopy. The resonance assigned to the hydride in **6a** is broad at 25 °C, but sharp at −45 °C, whilst that assigned to the hydride in **6b** is sharp at 25 °C and broad at −45 °C, thus indicating that the two compounds are involved in fluxional processes of different energies. The hydride in **6a** couples strongly with the PPh_2 phosphorus (41 Hz) and with one of the dppm phosphorus nuclei (14 Hz). These data are in accord with the solid state structure in which the dppm ligand is coordinated in an axial–apical arrangement (vide infra) and the hydride is bonded to same Ir atom of the axial dppm phosphorus. The hydride in isomer **6b** couples also with the second phosphorus of the dppm (7 Hz), which suggested that the two dppm phosphorus and the bridging hydride are bonded to the same Ir–Ir fragment.

The peak at δ −69.4 in the $^{31}P[^{1}H]$-NMR spectrum of **6a** was assigned to the apical dppm phosphorus (labelled P3 in the molecular structure discussed below), based on a chemical shift analysis (vide supra), which relates low frequency phosphorus chemical shifts to the apical position in substituted tetrahedral Ir clusters. The peak at δ −35.5 was assigned to radial dppm phosphorus (labelled P2) due to the large J_{P1-P2} (74 Hz) observed with the PPh_2 phosphorus, which reflects a *transoid* orientation of the nuclei. This assignment is supported by the similarity of the chemical shifts observed for the dppm phosphorus nuclei in radial and apical positions in $[Ir_4(CO)_8(dppm)_2]$, at δ −24.5 and −62.4, respectively [16,24] and in **6a**.

In the case of compound **6b**, the similarity between the chemical shifts of the two dppm phosphorus (δ −36.8 and −31.5) and that of the axial dppm phosphorus of **6a** (δ −35.5) suggests that the dppm phosphorus in **6b** bridge a Ir–Ir bond in an axial–axial arrangement. The structure proposed for isomer **6b** is shown schematically in Scheme 5, together with that of isomer **6a**. The structure of **6b** is similar to that established for $[Ir_4(CO)_{10}(dppm)]$ on the basis of VT multinuclear NMR studies [13] which contains two μ-CO ligands in place of the phosphide and hydride bridging ligands in **6b**.

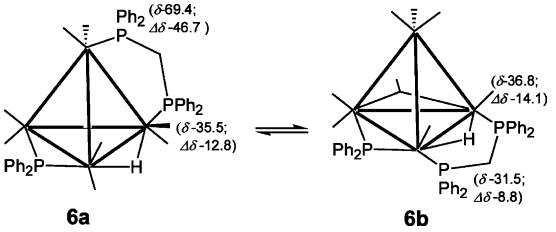

Scheme 5. Schematic structures of isomers **6a** and **6b**, which undergo interconversion.

It is clear that inter-conversion between isomers **6a** and **6b** involves migration of one of the phosphorus of the dppm ligand and rearrangement of the CO ligands. Similar process involving the diphosphine P–P = *cis*-$Ph_2PCH{=}CHPPh_2$ in $[Ir_4(CO)_{12-2n}(P{-}P)_n]$ was recently described in the literature by R. Roulet and coworkers [25].

2.3.1. Crystal and molecular structure of *6a*

Compound **6a** was crystallised from CH_2Cl_2–hexane and its structure, determined by an X-ray analysis, is shown in Fig. 3, together with the labelling scheme, and selected bond distances and angles, are shown in Table 4. The molecule consists of a distorted tetrahedral arrangement of Ir atoms with average Ir–Ir distance 2.742 Å, with a hydride and a phosphide ligands bridging two basal edges. The dppm ligand bridges an apex to base edge [Ir(1)–Ir(4) 2.701(1) Å] and all eight carbonyl ligands bond terminally, two to each iridium atom, in contrast to the structures of compounds **1**, **4** and **5c** which contain a bridging CO ligand on the third basal edge. In fact, **6a** is the first CO substitution derivative of **1** with only terminal CO ligands.

2.4. Synthesis and characterisation of $[HIr_4(CO)_8(dppen)(\mu\text{-}PPh_2)]$ (7)

The reaction of cluster **1** with one equivalent of dppen in CH_2Cl_2 at 30 °C leads to the formation of $[HIr_4(CO)_8(dppen)(\mu\text{-}PPh_2)]$ **7** in 50% yield, besides other decomposition products. The red compound **7** was characterised by spectroscopic (see Tables 1 and 2) and analytical methods.

The $^{31}P[^{1}H]$-NMR spectrum of **7** (Table 2) reveals a strong coupling between a dppen phosphorus nucleus and the PPh_2 phosphorus, suggesting that this phosphorus of the diphosphine ligand occupies a radial

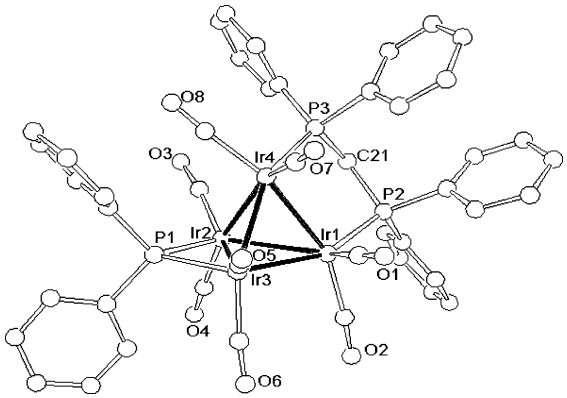

Fig. 3. Molecular structure of $[HIr_4(CO)_8(dppm)(\mu\text{-}PPh_2)]$ (**6a**).

position *trans* to the phosphido phosphorus, similar to the compound **6a**.

The coordination chemical shift for the two dppen phosphorus of **7** ($\Delta\delta$ 66.1 and 54.6) are close to those of the analogous $[Ir_4(CO)_{10}(dppen)]$ ($\Delta\delta$ 70.6 and 44.8) [25] and $[Ir_4(CO)_{10}(dmpe)]$ (dmpe = $Me_2P(CH_2)PMe_2$, $\Delta\delta$ 72.8 and 55.3), [13] which exhibit the diphosphine ligand bonded to an unique metal centre in the polyhedron. Based on this similarity, the structure of **7** was proposed, as shown in Scheme 6, with the phosphorus atoms of the dppen ligand occupying a radial and an axial positions of the same iridium atom, resulting in a five membered ring.

2.5. Synthesis and characterisation of $[\{HIr_4(CO)_9(\mu\text{-}PPh_2)\}_2(dppb)]$ (**8a**) and $[HIr_4(CO)_8(dppb)(\mu\text{-}PPh_2)]$ (**8b**)

The reaction of cluster **1** with one equivalent of dppb in CH_2Cl_2 at 30 °C leads to the formation of two red compounds **8a** (35%) and **8b** (25%), formulated as $[\{HIr_4(CO)_9(\mu\text{-}PPh_2)\}_2(dppb)]$ and $[HIr_4(CO)_8(dppb)(\mu\text{-}PPh_2)]$, respectively, based on IR and ^1H and ^{31}P-NMR spectroscopic data only.

The IR spectrum of **8a** in the ν_{CO} region is very similar to that of compound **4** (see Table 1) which indicates mono-substitution and, therefore, that this cluster possesses a dppb ligand bridging two '$HIr_4(CO)_9(\mu\text{-}PPh_2)$' units. The fact that the $^{31}P[^1H]$-NMR spectrum of **8a** is also very similar to that of compound **4** (see Table 2) suggests that the dppb is bonded to the base Ir atoms not associated with the PPh_2 ligand of the two Ir_4 units, in axial position, as shown in Scheme 6. The ^1H-NMR spectrum of **8a** also supports this formulation.

As the ν_{CO} bands of compound **8b** are shifted to lower frequencies by about 10 cm^{-1} with respect to those of compounds **8a** and **4**, compound **8b** must be more substituted than both species, and contain either a dppb ligand bonded to a single cluster via its two phosphorus atoms or, less probably, two dppm molecules bridging two Ir_4 clusters. The $^{31}P[^1H]$-NMR spectrum of **8b** exhibits a resonance at δ 261.1 (s), attributed to the phosphide phosphorus, and two singlets at δ 3.6 and 0.25, assigned to the dppb phosphorus nuclei, and whose chemical shift values are indicative of axial coordination. The structure of **8b** illustrated in Scheme 6 was confirmed by an X-Ray diffraction analysis (see below) that confirms the structure proposed for isomer **6b** of the dppm derivative (see Scheme 5).

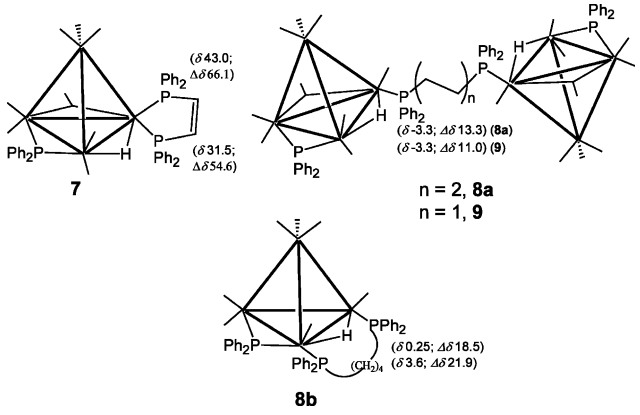

Scheme 6. Structures proposed for compounds **7**, **8a**, **8b** and **9**.

2.5.1. Crystal and molecular structure of **8b**

Compound **8b** was crystallised from CH_2Cl_2–hexane and its structure, determined by an X-ray analysis, is shown in Fig. 4, together with the labelling scheme, and selected bond distances and angles are given in Table 4. The molecule consists of a distorted tetrahedral arrangement of Ir atoms with average Ir–Ir distance 2.768 Å, similar to other derivatives of **1**, in which the basal edges are slightly longer than the apex to base edges. Compound **8b** exhibits the phosphorus atoms of the dppb ligand in different axial positions of the tetrahedron and bonded to the same iridium atoms that are bridged by the hydride ligand. Besides the bridging hydride, a μ-PPh_2 and a μ-CO groups form the basal plane of the cluster. Compound **8b** contains seven terminally bonded carbonyl groups, three to the apical iridium atom, one to each iridium atom bridged by the dppb ligand and two to the third basal Ir atom. This structure is similar to that of $[Ir_4(CO)_{10}(dppb)]$ [26] which contains two μ-CO ligands in place of the phosphide and hydride bridging ligands in **8b**. The dppb ligand in **8b** presents P–C–C and C–C–C angles [114.1(6), 113.1(6) and 109.8(6), 115.6(6)°, respectively], which, on average, are larger than expected for sp^3 hybridised atoms, whereas the P–C–P angle of 110.4(6)° in the dppm derivative, **6b**, is closer to the expected value. Thus, the increase in the hydrocarbon chain length leads to larger tensions in the Ir–P–C_n–P–Ir ring, which explains the preferential formation of the dimeric product upon reaction with dppe and, in the

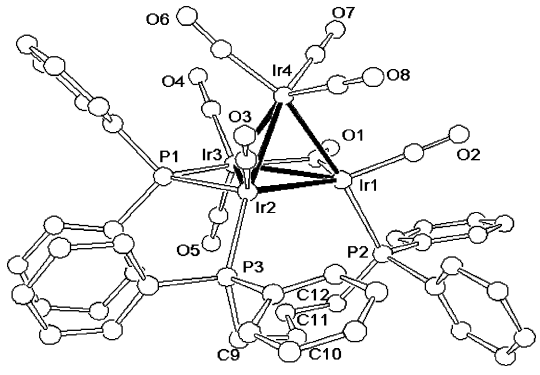

Fig. 4. Molecular structure of $[HIr_4(CO)_8(dppb)(\mu\text{-}PPh_2)]$ (**8a**).

case of that with dppb, formation of both dimeric and monomeric compounds (~7:5).

2.6. Synthesis and characterisation of [{$HIr_4(CO)_9(\mu$-$PPh_2)\}_2$(dppe)] (9)

The reaction of cluster **1** with one equivalent of dppe in CH_2Cl_2 at 30 °C leads to the formation of a single red product **9** (40%) which was formulated as [{$HIr_4(CO)_9(\mu$-$PPh_2)\}_2$(dppe)], on the basis of IR and ^1H and ^{31}P-NMR spectroscopic data only. The alternative route involving the use of DBU and CF_3COOH did not give better yield of this product.

The similarity of the IR and $^{31}P[^1H]$-NMR spectra of compounds **9**, **4** and **8a** (see Tables 1 and 2) strongly suggests that the structure of compound **8** is identical to that of dimer **8a**, shown in Scheme 6.

3. Conclusions

In summary, our work shows that it is possible to use the structural correlations previously established for the phosphine and diphosphine derivatives of $[Ir_4(CO)_{12}]$ on the basis of a combination of multinuclear NMR spectroscopy and X-ray diffraction studies, to propose structures for the phosphine derivatives of $[HIr_4(CO)_{10}(\mu$-$PPh_2)]$ (**1**) and in several cases, the NMR based structures were confirmed by X-ray structural analyses. These correlations were particularly useful, due to the number of isomers formed for both mono and di-substituted compounds and because of the possibility of isomerisation in solution. These NMR studies made it possible to monitor the formation of kinetic and thermodynamic products, as well as that of inter-converting isomers.

4. Experimental

Iridium carbonyl (Strem Chemicals), tetrabutylammonium bromide (Aldrich), silver hexafluoroantimonate (Aldrich), diphenylphosphine, trimethylphosphine, triphenylphosphine and bis(diphenilphosphine)methane were used as purchased; 1,8-diazabicyclo[5.4.0]undec-7-ene was distilled before use. Tetrahydrofuran was dried over sodium and benzophenone, dichloromethane over CaH_2, hexane and toluene over sodium. All solvents were freshly distilled and degassed before use. The compounds $[HIr_4(CO)_{10}(\mu$-$PPh_2)]$ (**1**), $[HIr_4(CO)_9(PPh_3)(\mu$-$PPh_2)]$ (**4**) and $[HIr_4(CO)_8(PPh_3)_2(\mu$-$PPh_2)]$ (**5**) were prepared by published methods [1]. The progress of the reactions was monitored by analytical TLC (precoated plates, silica gel F254, 0.25 mm thick; E. Merck), IR and NMR spectroscopy. The separation and purification of the reaction products was carried out by preparative TLC (2 mm thick glass plates 20 × 20 cm, silica gel GF 254; Fluka). The reactions and manipulations were performed in typical Schlenk systems, under inert atmosphere of argon. All Ir_4-clusters were stored under inert atmosphere to avoid some decomposition observed in some compounds stored for long time in the solid state. Samples of ^{13}CO enriched clusters (prepared from $NBu_4[Ir_4(CO)_{11}Br]$ were used for ^{13}C-NMR experiments.

Infrared spectra were recorded on a Bomem (FT-IR Michelson) spectrophotometer between 2200 and 1600 cm^{-1} (ν_{CO}), $^{31}P[^1H]$, ^1H and $^{13}C[^1H]$ spectra on a Bruker AC 300P spectrometer using, as references, 85% H_3PO_4 (external) for the former and $SiMe_4$ for the other nuclei and secondary ionization mass spectra (SIMS), on a VG AutospecFisons spectrometer operating at 25–30 kV (40 μA) with a xenon beam operating at 8 keV.

4.1. Preparation of $[HIr_4(CO)_9(PMe_3)(\mu$-$PPh_2)]$ (2) and $[HIr_4(CO)_8(PMe_3)_2(\mu$-$PPh_2)]$ (3)

To an orange solution of compound **1** (100 mg, 0.081 mmol) at room temperature (r.t.), in toluene (20 ml), a solution of PMe_3 (8.4 μl, 0.081 mmol), in toluene (10 ml) was added slowly, using a dropping funnel (about 1 h) and the mixture was left stirring for 3 h. The solvent was evaporated and the mixture separated by TLC with CH_2Cl_2–hexane (2:3) to yield unreacted **1** (15 mg), **2** (40 mg, 38%), **3** (30 mg, 28%) and some decomposition products. Compounds **2** and **3** were recrystallised from CH_2Cl_2–hexane to give red microcrystals. Anal. Calc. for $C_{24}H_{20}O_9P_2Ir_4$ (**2**): C, 22.5; H, 1.6; Found: C, 22.6; H, 1.4%. Anal. Calc. for $C_{26}H_{29}O_8P_3Ir_4$ (**3**): C, 23.5; H, 2.2; Found: C, 23.8; H, 2.3%.

4.2. Preparation of $[HIr_4(CO)_8(dppm)(\mu$-$PPh_2)]$ (6)

4.2.1. Method 1

A solution of dppm (31 mg, 0.081 mmol) in CH_2Cl_2 (5 ml) was added slowly to **1** (100 mg, 0.081 mmol) in CH_2Cl_2 (20 ml), as described above, and the mixture was kept stirring for about 2 h at 30 °C. The solvent was then evaporated under vacuum and the mixture purified by TLC, as described above, to yield two isomers of **6**, **6a** (red, $R_f = 0.69$, 33 mg, 30%) and **6b** (yellow, $R_f = 0.49$, 16 mg, 15%) and some decomposition on the base line. Attempts at recrystallising both isomers from CH_2Cl_2–hexane mixtures only resulted in crystals of **6a**. Anal. Calc. for $C_{45}H_{33}O_8P_3Ir_4$ (**6a**): C, 34.6; H, 2.1; Found: C, 32.9; H, 2.2%. SIMS (**6a**) 1564 $[M]^+ = M'$; 1508 $(M'-2CO)^+$; 1374 $(M'-4CO-PhH)^+$; 1346 $(M'-5CO-PhH)^+$.

4.2.2. Method 2

DBU (9.2 μl, 0.044 mmol) was added to a solution of **1** (70 mg, 0.056 mmol) in CH_2Cl_2 (20 ml), under quick stirring, at 30 °C. After stirring for 15 min. the mixture was cooled to −10 °C and a solution of dppm (21 mg, 0.056 mmol) in CH_2Cl_2 (5 ml) was added. The mixture was left stirring for 2 h, after which time CF_3COOH (4.7 μl, 0.061 mmol) was added to protonate the products. The solvent was evaporated under vacuum, and the mixture separated by TLC as described above to yield the same two isomers **6a** (40%) and **6b** (20%).

4.3. Preparation of $[HIr_4(CO)_8(dppen)(\mu\text{-}PPh_2)]$ (7)

4.3.1. Method 1

These compounds were prepared as described in method 1 for **6a** and **6b**, from **1** (55 mg, 0.044 mmol) and dppen (18 mg, 0.044 mmol) in CH_2Cl_2 (10 ml). The mixture was left stirring for 6 h and separated as described for **6a** and **6b**. Compound **7** (red, $R_f = 0.55$, 50%) and the starting material **1** (20%) were isolated and compound **7** was recrystallised from CH_2Cl_2–hexane at 4 °C. Anal. Calc. for $C_{47}H_{33}O_8P_3Ir_4$ (**7**): C 35.1, H 2.1; Found: C, 35.4; H, 2.4%. SIMS (**7**) 1576 $[M]^+ = M'$; 1548 $(M'-1CO)^+$; 1520 $(M'-2CO)^+$; 1492 $(M'-3CO)^+$; 1414 $(M'-3CO-PhH)^+$.

4.3.2. Method 2

These compounds were prepared as described in method 2 for **6a** and **6b**, from **1** (55 mg, 0.044 mmol), DBU (8.5 μl, 0.057), dppen (18 mg, 0.044 mmol) and CF_3COOH (4.7 μl, 0.061 mmol). Compound **7** (red, $R_f = 0.55$, 60%) and the starting material **1** (15%) were isolated.

4.4. Preparation of $[\{HIr_4(CO)_9(\mu\text{-}PPh_2)\}_2(dppb)]$ (8a) and $[HIr_4(CO)_8(dppb)(\mu\text{-}PPh_2)]$ (8b)

4.4.1. Method 1

These compounds were prepared as described in method 1 for **6a** and **6b**, from **1** (55 mg, 0.044 mmol) and dppb (19 mg, 0.044 mmol) in CH_2Cl_2 (10 ml). The mixture was left stirring for 7 h and separated as described for **6a** and **6b**. Compounds **8a** (red, $R_f =$ 0.53, 35%), **8b** (red, $R_f = 0.37$, 25%) and the starting material **1** (10%) were isolated and compounds **8a** and **8b** recrystallised from CH_2Cl_2–hexane at 4 °C. Anal. Calc. for $C_{70}H_{50}O_{18}P_4Ir_8.0.5C_6H_{14}$ (**8a**): C, 30.3; H, 2.0%; Found: C, 30.3; H, 2.1%. Anal. Calc. for $C_{48}H_{39}O_8P_3Ir_4$ (**8b**): C, 35.9; H, 2.5; Found: C, 33.5; and H, 2.6%. SIMS (**8b**) 1606 $[M]^+ = M'$; 1578 $(M'-1CO)^+$; 1550 $(M'-2CO)^+$; 1444 $(M'-3CO-PhH)^+$.

4.4.2. Method 2

These compounds were prepared as described in method 2 for **6a** and **6b**, from **1** (55 mg, 0.044 mmol), DBU (8.5 μl, 0.057), dppb (19 mg, 0.044 mmol) and CF_3COOH (4.7 μl, 0.061 mmol). Compound **8a** (red, $R_f = 0.53$, 35%), **8b** (red, $R_f = 0.37$, 25%) and the starting material **1** (15%) were isolated.

4.5. Preparation of $[\{HIr_4(CO)_9(\mu\text{-}PPh_2)\}_2(dppe)]$ (9)

4.5.1. Method 1

This compound was prepared as described in method 1 for **6a** and **6b**, from **1** (55 mg, 0.044 mmol) and dppe (18 mg, 0.044 mmol) in CH_2Cl_2 (10 ml). The mixture was left stirring for 7 h and separated as described for **6a** and **6b**. Compounds **9** (red, $R_f = 0.53$, 30%) and the starting material **1** (20%) were isolated and compound **9** was recrystallised from CH_2Cl_2–hexane at 4 °C.

4.5.2. Method 2

This compound was prepared as described in method 2 for **6a** and **6b**, from **1** (55 mg, 0.044 mmol), DBU (8.5 μl, 0.057), dppe (18 mg, 0.044 mmol) and CF_3COOH (4.7 μl, 0.061 mmol). Compounds **9** and **1** were isolated in the same yields as in method 1. Anal. Calc. for $C_{68}H_{46}O_{18}P_4Ir_8.0.5C_6H_{14}$ (**9**): C, 29.9; H, 1.9; Found: C, 29.9; H, 2.4%.

Table 5
Crystal data and details of measurements for compounds **5c**, **6a** and **8b**

	5c	**6a**	**8b**
Formula	$C_{56}H_{41}Ir_4O_8P_3$	$C_{45}H_{33}Ir_4O_8P_3$	$C_{49}H_{41}Ir_4O_8P_3$
Crystal size (mm)	0.20 × 0.16 × 0.14	0.18 × 0.18 × 0.12	0.16 × 0.14 × 0.10
Crystal system	Triclinic	Monoclinic	Triclinic
Space group	$P\bar{1}$	$P2_1/m$	$P\bar{1}$
a (Å)	10.766(3)	11.803(8)	11.437(4)
b (Å)	13.682(4)	10.727(3)	15.213(10)
c (Å)	21.777(6)	34.990(10)	15.978(10)
α (°)	73.58(2)	90	73.15(7)
β (°)	87.89(2)	96.53(4)	70.87(5)
γ (°)	66.95	90	89.24(6)
V (Å^3)	2821(1)	4401(4)	2503(2)
Z	2	4	4
D_{calc} (g cm^{-3})	2.005	2.358	2.243
μ (mm^{-1})	9.539	12.217	10.852
θ Range (°)	3–25	3–25	3–23
Reflections collected	9685	7829	7218
R_1 (on F, $I > 2\sigma(I)$)	0.0399	0.0411	0.0286
wR_2 (on F^2, all data)	0.1182	0.0910	0.0782

4.6. X-ray crystallographic determination of **5c**, **6a** and **8b**

Crystal data for all compounds were collected on a Nonius CAD4 diffractometer equipped with a graphite monochromator an Oxford Cryostream liquid-N_2 device. Crystal data and details of measurements are summarised in Table 5. Common to all compounds: Mo–K_α radiation, $\lambda = 0.71073$ Å, monochromator graphite. SHELXS-97 and SHELXL-97 [27] were used for structure solution and refinement based on F^2. Non-hydrogen atoms were refined anisotropically. Hydrogen atoms bound to carbon atoms were added in calculated positions. SCHAKAL-99 [28] was used for the graphical representation of the results.

5. Supplementary crystallographic data

Crystallographic data (excluding structure factors) for the structures in this paper have been deposited with the Cambridge Crystallographic Data Centre as supplementary publications numbers CCDC 178435 (**5c**), 178434 (**6a**) and 178436 (**8b**). Copies of the data can be obtained, free of charge from The Director, CCDC, 12 Union Road, Cambridge CB2 1EZ, UK (Fax: +44-1223-336033; e-mail: deposit@ccdc.cam.ac.uk or http://www.ccd.cam.ac.uk/conts/retrieving.html.

Acknowledgements

We acknowledge financial support from the Commission of European Communities, Conselho Nacional de Pesquisas Científicas e Tecnológicas (CNPq), Fundação de Amparo à Pesquisa do Estado de São Paulo (FAPESP) and PADCT (Brazil).

References

[1] F.S. Livotto, P.R. Raithby, M.D. Vargas, J. Chem. Soc. Dalton Trans. (1993) 1797.
[2] P.B. Hitchcock, J.F. Nixon, M.D. Vargas, C.M. Ziglio, J. Chem. Soc. Dalton Trans. (2000) 2527.
[3] M.D. Vargas, C.M. Ziglio, J.F. Nixon, D. Braga, F. Grepioni, manuscript in preparation.
[4] M.D. Vargas, C.M. Ziglio, D. Braga, F. Grepioni, J. Braz. Chem. Soc. (2002) submitted for publication.
[5] M.H. Araujo, Ph.D. thesis, Universidade Estadual de Campinas, Brazil, 1995.
[6] (a) M.D. Vargas, R.M.S. Pereira, D. Braga, F. Grepioni, J. Chem. Soc. Chem. Commun. (1993) 1008;
(b) M.D. Vargas, R.M.S. Pereira, D. Braga, F. Grepioni, J. Braz. Chem. Soc. 10 (1999) 35.
[7] M.H.A. Benvenutti, M.D. Vargas, D. Braga, F. Grepioni, E. Parisini, B.E. Mann, Organometallics 12 (1993) 2955.
[8] M.H.A. Benvenutti, M.D. Vargas, D. Braga, F. Grepioni, B.E. Mann, S. Naylor, Organometallics 12 (1993) 2947.
[9] (a) M.H.A. Benvenutti, P.B. Hitchcock, J.F. Nixon, M.D. Vargas, J. Chem. Soc. Chem. Commun. (1994) 1869;
(b) M.H. Araujo, P.B. Hitchcock, J.F. Nixon, M.D. Vargas, J. Braz. Chem. Soc. 9 (1998) 563.
[10] L.A.P. Kane-Maguire, P.R. Raithby, E. Sinn, M.D. Vargas, ACS Abstracts, 194, 320-INOR, August 30 (1987).
[11] G.F. Stuntz, J.R. Sharpley, J. Am. Chem. Soc. (1977) 607.
[12] B.E. Mann, C.M. Spencer, A.K. Smith, J. Organomet. Chem. 247 (1983) C17.
[13] R. Ros, A. Scrivanti, V.G. Albano, D. Braga, L. Garlaschelli, J. Chem. Soc. Dalton Trans. (1986) 2411.
[14] B.E. Mann, M.D. Vargas, R. Khattar, J. Chem. Soc. Dalton Trans. (1992) 1725.
[15] D. Braga, F. Grepioni, G. Guadalupi, A. Scrivanti, R. Ros, R. Roulet, Organometallics 6 (1987) 56.
[16] A. Strawczynski, C. Hall, G. Bondietti, R. Ros, R. Roulet, Helv. Chim. Acta 77 (1994) 754.
[17] Y. Chi, H.-F. Hsu, L.-K. Liu, S.-M. Peng, G.-H. Lee, Organometallics 11 (1992) 1763.
[18] A.M. Bradford, M.C. Jenings, R.J. Puddephatt, Organometallics 7 (1988) 792.
[19] A.M. Bradford, G. Douglas, L.J. Manojlovic-Muir, K.W. Muir, R.J. Puddephatt, Organometallics 9 (1990) 409.
[20] R. Ramachandran, D.-S. Yang, N.C. Payne, R.J. Puddephatt, Inorg. Chem. 31 (1992) 4237.
[21] S. Ching, D.F. Shriver, J. Am. Chem. Soc. 111 (1989) 3243.
[22] G. Bondietti, G. Laurenczy, R. Ros, R. Roulet, Helv. Chim. Acta 77 (1994) 1869.
[23] G. Laurenczy, G. Bondietti, A.E. Merbach, B. Moulet, R. Roulet, Helv. Chim. Acta 77 (1994) 547.
[24] D.F. Foster, B.S. Nicholls, A.K. Smith, J. Organomet. Chem. 236 (1982) 395.
[25] G. Laurenczy, G. Bondietti, R. Ros, R. Roulet, Inorg. Chim. Acta 247 (1996) 65.
[26] A. Strawczynsky, R. Ros, R. Roulet, D. Braga, C. Gradella, F. Grepioni, Inorg. Chim. Acta 170 (1990) 17.
[27] G.M. Sheldrick, SHELXL97, Program for Crystal Structure Determination, University of Göttingen, Göttingen, Germany, 1997.
[28] E. Keller, SCHAKAL99 Graphical Representation of Molecular Models, University of Freiburg, Germany, 1999.